Selective hydrogenation of vanillin to vanillyl alcohol over Pd, Pt, and Au catalysts supported on an advanced nitrogen-containing carbon material produced from food waste

Xingjie Guo[a,b], Ge Gao[a,b], Javier Remón[c*], Ya Ma[a,b], Zhicheng Jiang[a,b*], Bi Shi[a,b], Daniel C.W. Tsang[d,e]

[a] Department of Biomass Science and Engineering, Sichuan University, Chengdu, 610065, P. R. China

[b] National Engineering Research Center of Clean Technology in Leather Industry, Sichuan University, Chengdu, 610065, P. R. China

[c] Instituto de Carboquímica, CSIC, Zaragoza, 50018, Spain

[d] Department of Civil and Environmental Engineering, The Hong Kong Polytechnic University, Hung Hom, Kowloon, Hong Kong, P. R. China

[e] Research Institute for Future Food, The Hong Kong Polytechnic University, Hung Hom, Kowloon, Hong Kong, P. R. China

*Email: jremon@icb.csic.es; zhichengjiang@scu.edu.cn

Abstract:

Food waste worldwide has been threatening the environment and resulting in high carbon emissions. Although anaerobic fermentation is a potential solution transforming food waste into valuable chemicals, a large amount of the fermentation residue remains as solid waste. For closing the circular economy loop for food waste valorization, we proposed a thermo-chemical activation of a fermentation residue produced from a mixture of food waste and sludge to prepare a nitrogen-enriched, advanced carbon material. This could be used as a support to synthesize Pd/C, Pt/C and Au/C catalysts for the aqueous-phase hydrogenation of vanillin to vanillyl alcohol at mild reaction conditions. The produced alcohol increased sixfold the commercial value of the original aldehyde. The catalytic performance (based on the vanillin conversion and vanillyl alcohol yield) followed the order of Pd/C > Pt/C > Au/C. The Pd/C catalyst showed an excellent catalytic activity (>99% vanillin conversion and >99% vanillyl alcohol selectivity) at optimized reaction conditions (i.e., 30 ºC and 0.7 MPa H_2 for 90 min, with 2 mmol vanillin/10 mg catalyst), along with high reusability and stability (up to four consecutive runs). These catalytic features outperformed those of a commercial Pd/C catalyst owing to: (i) high reduction degree and stabilization of the Pd particles on the carbon support, which accommodated a higher proportion of pyridinic than pyrrolic nitrogen, and (ii) rapid adsorption of the aldehyde group on the catalyst combined with rapid desorption of the newly formed hydroxymethyl group. This exceptional catalytic behavior was corroborated by efficient hydrogenation of other lignin-derived aromatic aldehydes, including p-hydroxybenzaldehyde and syringaldehyde, to their respective alcohols. Our results can bring a

novel use for food waste in catalysis and represent a sustainable and efficient conversion of biomass into value-added chemicals and advanced materials.

Keywords:

food waste; fermentation residue; activated carbon; catalytic hydrogenation; engineered biochar; sustainable waste management

1 Introduction

Food waste production has significantly risen over the past few years. It is estimated that 4.16 billion tons of food waste will be produced annually in 2025. This implies an increase of around 50% in 20 years, compared to 2.78 billion tons of food waste disposal in 2005 [1]. Food waste primarily results from households, canteens, restaurants, and industrial food processing plants. It comprises biomass-based carbohydrates, proteins, oils, lignin and inorganic salts [2]. In view of environmental concerns and governmental policies, new processes and valorization strategies are being sought for the sustainable management and disposal of food waste [3,4].

Efficient valorization of the organic matrix in food waste into value-added chemicals and functional materials not only benefits the recycling of food waste but also helps achieve the reduction target of carbon emissions [5,6]. Anaerobic fermentation has been widely investigated

to convert food waste into high-value products [7-10]. This process involves the degradation of the organic components in food waste with microorganisms under anaerobic conditions, resulting in gaseous (methane and hydrogen) and liquid (carboxylic acids) products. However, the major bottleneck is that the vast majority of food waste remains as a residue in a solid state [11,12]. As such, it is crucial to develop alternative uses for the valorization of this food waste fermentation residue (FWFR) to close the loop [13,14]. An up-and-coming option for the valorization of the FWFR is the production of advanced carbon materials, particularly for activated carbon, engineered biochar and hydrochar, which can be applied in many applications, including soil conditioners, pollutant adsorbents, and catalyst supports [15-17].

Among these applications, using biomass-derived carbon materials in catalysis has attracted significant attention [18,19]. The porous structure, high specific surface area, and excellent adsorption capabilities make them appropriate for developing renewable and carbon-supported metal catalysts for various catalytic processes [20,21]. However, achieving good metal dispersion onto the carbon material with high metal loadings is challenging. Heteroatom doping has been widely adopted, mainly nitrogen, onto the carbon material [22,23]. Such a modification increases its defects and disorder, facilitating the subsequent dispersion of metals and offering more active sites for catalysis [24,25]. For example, Zhou et al. [26] prepared a nitrogen-doped activated carbon through the pyrolysis of industry paper sludge with melamine, which showed superior electroconductivity and strong reduction ability to Cr (VI). Peng et al. [27] synthesized nitrogen-doped carbon nanosheets by mixing pomelo mesocarps and urea in ethanol, followed by a high-

temperature carbonization step, to prepare supercapacitors. These publications highlight the high potential of nitrogen doping to enhance the physicochemical properties of carbon materials produced from lignocellulosic biomass. Still, an external nitrogen source was needed except for a few nitrogen-containing biomasses, such as chitosan and seaweed. In contrast to lignocellulosic biomass, the FWFR contains a much higher N/C ratio, which makes it an excellent candidate for preparing nitrogen-enriched activated carbon or engineered biochar without the need for blending pretreatments.

Given this background, this works addresses the first-time preparation of metal/N-C supported catalysts from a FWFR produced from the anaerobic fermentation of a solid mixture containing food waste and sludge. Three typical metal nanoparticles (Pd, Pt, and Au) were immobilized on the FWFR-derived carbon catalysts, which were thoroughly characterized, studying their morphology, metallic crystalline structures, distributions of metal valence states, and defect degrees. Then, these catalysts were evaluated for the catalytic hydrogenation of vanillin, one of the main products from the oxidative degradation of lignin [28]. This transformation involves converting the aldehyde group to a hydroxymethyl and a methyl group and converting the benzene ring to a cyclohexane [29]. The vanillin conversion is challenging due to the high number of side reactions, leading to different hydrogenated products. Among these, vanillyl alcohol is the most desirable owing to its high commercial value and wide use in the pharmaceutical industry [30]. However, very few studies have focused on the hydrogenation of vanillin to produce vanillyl alcohol, owing to the diverse side reactions. In particular, Duan et al. [31] used a Ni-Co-P/HAP

catalyst in the hydrodeoxygenation of vanillin and found that after 3 h reaction at 200 ℃, the main product was creosol, while the selectivity of vanillyl alcohol was less than 10%. Alijani et al. [32] used a Pd-activated carbon catalyst for the hydrodeoxygenation of vanillin. They achieved a selectivity to vanillyl alcohol below 80% at a reaction temperature of 50 ℃. Therefore, in this work, we have developed novel Pd/C, Pt/C and Au/C catalysts for this reaction. The experiments were conducted over a wide range of reaction conditions for achieving a high selectivity to vanillyl alcohol. Once the process was optimized, the stability and recyclability of the catalysts were evaluated to illustrate the potential industrial application of these novel catalysts. The new knowledge of this work will represent a landmark achievement in the fields of catalytic biorefinery and sustainable waste management.

2 Experimental Section

2.1 Materials

Food waste, whose main constituents are 50% rice, 30% meat, and 20% vegetables, was collected from the canteen of Sichuan University in Chengdu (China). Sludge was obtained from a sludge storage tank at Chengdu Huayang Sewage Treatment Plant (Chengdu, China). The most representative properties of the sludge used in the experiment are listed in Table S1. K_2PdCl_4, $HPtCl_6 \cdot 6H_2O$, $HAuCl_4 \cdot 3H_2O$, vanillyl alcohol and creosol were purchased from Aladdin Biochemical Technology Co., Ltd (Shanghai, China). Vanillin was acquired from J&K Scientific

Co., Ltd (Beijing, China). Polyvinyl pyrrolidone (PVP) was obtained from Macklin Biochemical Co., Ltd (Shanghai, China), while Glycine was bought from Titan Scientific Co., Ltd (Shanghai, China). All the chemicals were used as received without further purification.

2.2 Catalysts synthesis

The synthesis of the catalysts comprises three steps: i.) the preparation of the support, ii.) their thermal and chemical activation, and iii.) the incorporation of the active metals on the solid produced. For the former, the food waste was firstly crushed into a uniform emulsion and mixed with sludge at a dry mass ratio of 9:1. Then water was added to obtain a 20 g/L mixture according to a conventional anaerobic fermentation process reported in the literature [33]. After adjusting the pH value of the mixture at 8 with sodium hydroxide, the anaerobic fermentation was carried out at room temperature for 8 days. According to the literatures, the anaerobic fermentation of food waste with sludge is efficient at pH 8, as this medium provides a high conversion to volatile fatty acids [33,34]. Therefore, this pH was used to maximize the conversion and obtain a recalcitrant solid (fermentation) residue. Afterward, the fermentation mixture was centrifuged to remove the supernatant and washed with ethanol and deionized water. Then, the remaining fermentation solid residue was dried at 80 ℃ to obtain the FWFR. In the second step, the FWFR was first subjected to a thermal treatment in a tubular furnace at 450 °C for 2 h under nitrogen gas (20 mL STP/min flow rate). Subsequently, the obtained biochar was ground into small particles and chemically activated with KOH. For the activation, the biochar was soaked with a KOH solution (4 M) for 12

h, using a KOH solution/biochar ratio of 4 mL/g. Then, water was removed in an oven at 105 ºC. Subsequently, the pretreated biochar was subjected to another thermal treatment in a tubular furnace at 800 °C for 2 h under a nitrogen atmosphere (20 mL STP/min flow rate). After cooling to room temperature, the solid residue was washed with deionized water until the pH value was nearly 7 and dried to obtain the activated carbon. Prior to the impregnation step, Pd, Pt and Au metal nanoparticles were synthesized. For this, a PVP/Glycine (stabilizer and reducing agent, respectively) solution and a metal cation solution, containing either K_2PdCl_4, $HPtCl_6 \cdot 6H_2O$ or $HAuCl_4 \cdot 3H_2O$, were mixed in a pressurized tube (the metal concentration was 1.7 g/L), with the tube being immersed in an oil bath at 180 °C for 2 h. Each metal suspension was then mixed with the activated carbon support (mass ratio of metal to carbon support equals 1.5 : 98.5) and stirred at room temperature for 2 h in a beaker to ensure the metal particles adsorbed on the activated carbon support. In all the cases, the amounts of precursors were in excess (three times higher) with respect to the theoretical values, as our previous experience showed that part of these metal particles could adhere to the wall of reaction tubes during the synthesis. After removing the liquid fraction in an oven at 105 ºC, the solid fraction was calcined in a tubular furnace under a closed air atmosphere at 400 ºC for 1 h. This methodology allows synthesizing metal (c.a. 1 wt%) supported catalysts of Pd/C, Pt/C and Au/C (Table S2).

2.3 Characterization of the solid samples

The elemental composition of the FWFR was determined by elemental analysis, using a Vario EL cube-Elementar analyzer, and inductively coupled plasma atomic emission spectroscopy (ICP-AES) on a 5100SVDV, Agilent Technologies apparatus. The chemical groups in the FWFR were determined by Fourier Transform Infrared Spectroscopy (FT-IR) on a Nicolet iS50, Thermo Fisher. The fiber analysis was determined using the Vanset chemical titration (for cellulose, hemicellulose, lignin and starch) and the Kjeldahl method (to calculate the protein content according to the amount of N in the sample). The activated carbon and prepared catalysts were characterized by X-ray diffraction (XRD), N_2 isotherm adsorption-desorption, transmission electron microscope (TEM), X-ray photoelectron spectroscopy (XPS) and Raman spectrometry. XRD spectra were obtained from Bruker AXS D8 Advance X-ray diffractometer with Cu Kα as the X-ray source (λ = 1.54056 Å, 40 KV, 40 mA), while the N_2 isotherm adsorption-desorption curves were acquired on a Micromeritics ASAP 2460. TEM images were obtained by a Thermo Fisher Scientific Talos F200S TEM and XPS analyses were conducted on a Thermo Fisher Scientific ESCALAB Xi^+ X-ray photoelectron spectrometer, with the results calibrated with C_{1S} binding energy at 284.8 eV. The Raman spectra were obtained on a Thermo Fisher Scientific DXRxi Raman spectrometer, with an excitation wavelength of 532 nm and a wavenumber in the range of 1000-3000 cm^{-1}. The catalyst metal loading was measured by inductively coupled plasma atomic emission spectroscopy (ICP-AES) on a 5100SVDV, Agilent Technologies apparatus.

2.4 Catalytic hydrogenation of vanillin

The catalytic experiments were carried out in a 50 mL stainless steel autoclave reactor equipped with a mechanical stirrer and an inner thermocouple (Shijisenlang, China). For a typical run, 2 mmol vanillin, 50 mg catalyst and 20 mL deionized water were placed in the air-tight reactor. Before the pressure of the reactor was pressurized at 2 MPa (experimental conditions), the inner atmosphere was purged 5 times with H_2 to remove the air. Then, the reactor was heated to 60 ºC in a furnace and held for 2 h, with 500 rpm of mechanical stirring. After the reaction was completed, the catalyst was separated from the reaction mixture by filtration. First, the reaction solution was analyzed by gas chromatography-mass spectrometry (GC-MS) (6890N-GCMS, Agilent) to identify the reaction products. Then, these were quantitatively determined by gas chromatography with a flame ionization detector (GC-FID) (Clarus 580, PerkinElmer) to calculate the conversion and yields of the products. In order to verify the purity of the hydrogenated products, the liquid effluent was analyzed by solution-state nuclear magnetic resonance spectroscopy on a Bruker AV II-400 MHz, examining the spectra of vanillin, vanillyl alcohol, and the other hydrogenated species produced.

In this work, the vanillin conversion and the yield of products were calculated by equations 1 and 2, respectively.

$$\text{Conversion (\%)} = (n_{\text{initial vanillin}} - n_{\text{remained vanillin}}) / n_{\text{initial vanillin}} \times 100\% \quad (1)$$

$$\text{Yield (\%)} = n_{\text{product}} / n_{\text{initial vanillin}} \times 100\% \quad (2)$$

where $n_{initial\ vanillin}$ represents the moles of initial vanillin used in the reaction, $n_{remaining\ vanillin}$ accounts for the moles of the remained vanillin after the reaction, and the $n_{product}$ is the moles of each product generated in the reaction.

2.5 Adsorption performance of the activated carbon and Pd/C

The adsorption performance of the Pd/C catalyst was measured by ultraviolet spectroscopy (UV 1800 BPC spectrophotometry). Vanillin, vanillyl alcohol and guaiacol were used to evaluate the adsorption properties of Pd/C. Three different aqueous solutions containing each one of these chemicals were prepared. Then, the same amount of the Pd/C catalyst was added to each solution to assess the adsorption of each species on the catalyst individually. After stirring to dissolve the liquid species in the aqueous medium, the concentrations of the chemicals in the solution were determined by ultraviolet spectroscopy, and the time-relative concentration (t-c) curve was evaluated for each chemical.

3 Results and discussion

3.1 Composition of the FWFR produced by fermentation

A solid material comprising a food waste and sludge mixture was used as the feedstock. As the fermentation process advanced, the color of the fermentation liquid and the solid fraction gradually

darkened, leading to the production of a gray-yellow suspension, with a solid content (i.e., FWFR) of 42.8%. The elemental analysis of this FWFR (Fig. 1a) shows a total organic content (C, H, O and N) of 90.4%, with C and O being the most abundant elements. The inorganic fraction primarily consists of 4.5% of Si, 1.1% of Al, and 0.6% of Fe. Figure 1b plots the fiber composition of the material, showing that starch is the most abundant organic component in FWFR, with a relative amount of 41.8%, followed by proteins with a proportion of 25%. The high starch content can be attributed to an incomplete fermentation of rice, which might exist as amylopectin with a higher degree of polymerization, while the protein content might reflect the presence of meat and beans in the food waste. The FWFR contains 14.6% lignocellulose, derived from vegetables in food waste. Specifically, cellulose, lignin, and hemicellulose contents are 5.5%, 7.5%, and 1.6%, respectively. As lignocellulosic biomass contains more cellulose than lignin [35,36], the lower amount of the former in the FWFR indicates that polysaccharides are more readily biodegraded during fermentation, resulting in a FWFR solid residue with a more significant proportion of lignin. The cellulose content of this residue is crystalline, as revealed by the broad signal peak was in the XRD spectrum at $2\theta = 15°\text{-}25°$ (Fig. 1c). Such a development indicates that amorphous cellulose is more readily biodegraded into liquid species than crystalline cellulose, which increases the proportion of this latter in the FWFR. These results agree with the FT-IR spectrum of the FWFR (Fig. 1d). The O-H and N-H signal peaks are respectively attributed to the polysaccharide and protein components in the fermentation residue, with the C=O signal peak being attributed to the acetyl group in hemicellulose. The characteristic diffraction peaks of SiO_2 and Al_2O_3 and the signal

peaks of Si, Al, and Fe oxides are also observed in the XRD pattern and FT-IR spectrum, which confirm the presence of metal oxides in the FWFR.

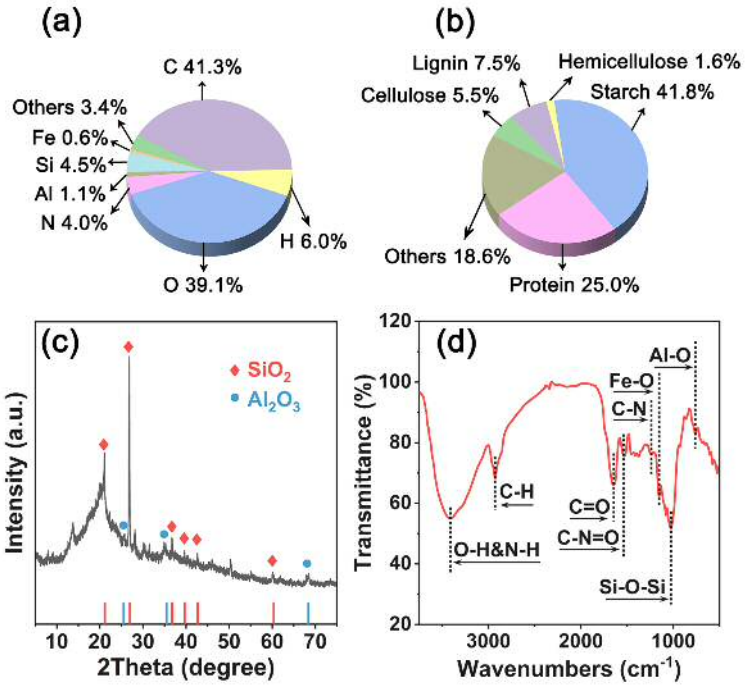

Figure 1. Characterization of FWFR. (a. Element analysis; b. Contents of organic components; c. XRD pattern; d. FT-IR spectrum)

3.2 Structural features of the catalysts

As a carbon-rich and nitrogen-containing source, the FWFR was converted to a N-doping activated carbon support and used to prepare metal-loaded catalysts. The N_2 isotherm adsorption-desorption analysis (Fig. 2) reveals that the specific surface area of the activated carbon is 1315.51 m^2/g, with a pore volume of 0.61 cm^3/g and an average pore diameter of 1.82 nm (Table 1). After the metal loading on the activated carbon, the specific surface areas of the Pd/C, Pt/C, and Au/C catalysts

were reduced to 895.81, 1066.72, and 1023.31 m^2/g, respectively. These diminishments were accompanied by decreases in their pore volumes (Table 1). This is because the metal nanoparticles occupy part of the internal pores and channels of the activated carbon. Besides, ICP analysis reveals that there are no statistically significant differences in the metal loading, i.e., around 1 wt% for the three catalysts synthesized (Table S2).

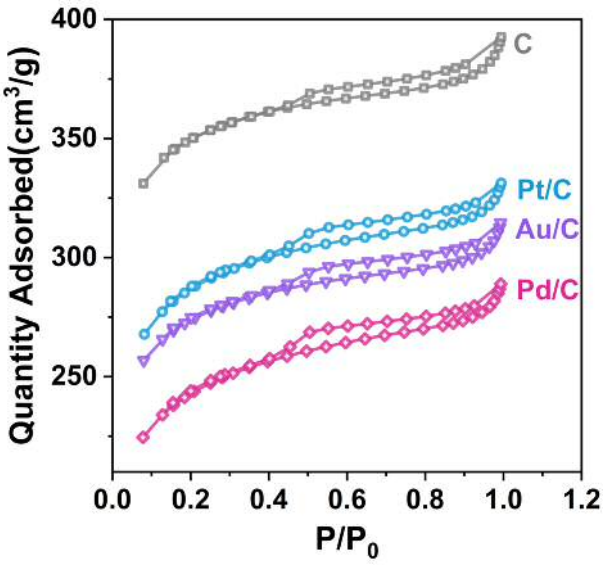

Figure 2. N_2 isotherm adsorption-desorption curves of Pd/C, Pt/C, Au/C, and C.

Table 1. BET analysis of Pd/C, Pt/C, Au/C, and C.

Catalyst	Surface area (m^2/g)	Pore volumes (cm^3/g)	Average pore width (nm)
C	1315.51	0.61	1.82
Pd/C	895.81	0.45	1.96
Pt/C	1064.72	0.51	1.89

Au/C	1023.31	0.49	1.86

After the metal loading, the TEM analysis (Fig. 3) reveals that the three catalysts have sheet-like structures comprising amorphous carbon, with the metal particles well-dispersed on the carbon supports. EDX-mapping demonstrates that the black spots appearing in the TEM images, especially for Pt/C, are attributed to the convolution carbon support layers (Fig. S1). The sizes of these metal particles differ, which is possibly ascribed to the different reduction behaviors of the metal ions with variable reduction potentials. In particular, the particle size of Pt is primarily distributed within the range of 2-3 nm, with an average particle size of 2.8 nm. In comparison, Pd and Au species are more easily reduced and aggregated into larger particles. For example, the particle size of Pd is distributed in a broad range of 5-65 nm, with an average particle size of 33.5 nm. Notably, the larger Pd particles on the Pd/C catalyst blocked the pore structure of the activated carbon support to a more significant extent. This resulted in a more pronounced decrease in the surface area of the catalyst in comparison to the original carbon support for the Pd/C catalyst than that observed for the other two catalysts.

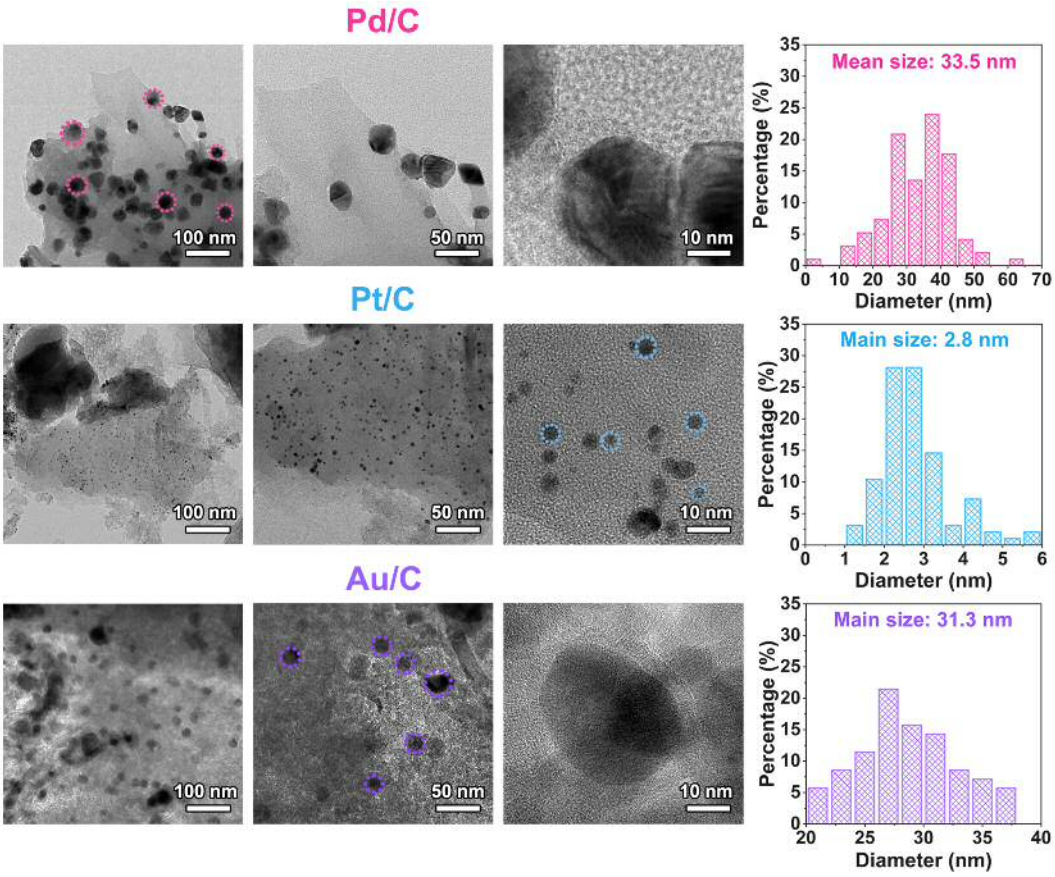

Figure 3. TEM images of Pd/C, Pt/C, and Au/C.

The crystalline phases and the valence states of the metal particles on the activated carbon materials were determined by XRD and XPS (Fig. 4). For the Pd/C catalyst, four diffraction peaks at 2θ = 40.1°, 46.6°, 68.1°, and 82.1° are observed, assigned to the (111), (200), (220) and (311) crystal planes of Pd, respectively. (JCPDS card No. 46-1043) [37]. The diffraction peak for the (101) crystal plane of PdO is also observed at 2θ = 33.9° (JCPDS card No. 41-1107). The XPS spectrum of Pd 3d can be divided into Pd^0 $3d_{5/2}$ (336.9 eV), Pd^0 $3d_{3/2}$ (342.2 eV), Pd^{2+} $3d_{5/2}$ (338.4 eV), and Pd^{2+} $3d_{3/2}$ (344.0 eV). This allows calculating the relative contents of Pd^0 (73.5%) and Pd^{2+} (26.5%), indicating that most of the Pd species were reduced to Pd^0 [38]. In the case of the Pt/C catalyst, diffraction peaks for Pt diffraction peak ((111) crystal plane, JCPDS card No. 04-

0802) and PtO ((222) crystal plane, JCPDS card No. 47-1171) are observed, while the Au/C catalyst only shows signals for Au crystal planes ((111), (200), (220) and (311), JCPDS card No. 04-0784) [39,40]. The diffraction peaks of SiO_2 or Al_2O_3 are detected in the XRD patterns of the three catalysts. These species derive from the initial sludge after being subjected to the carbonization process. The XRD patterns of the activated carbon support are shown in Fig. S2. For the latter two catalysts, the XPS analyses show that the proportion of Pt^0 in the Pt/C catalyst accounts for 49% of the total Pt, whereas Au^0 represents 100% of the Au species in the Au/C catalyst [41,42]. These results confirm that the reduction degrees of these metal species follow the order of: Pt < Pd < Au, and are highly correlated to their reduction potentials.

In addition to metal species, it has been widely reported that the presence of different forms of N species in carbon-supported catalysts affects their catalytic activity. N1s spectra can be deconvoluted into three peaks: pyridinic N, pyrrolic N, and quaternary N, respectively. However, the N1s spectra of our material do not adequately fit three peaks, while a perfect fit is achieved considering the contribution of pyridinic N and pyrrolic N only. These data indicate that N is present in the form of pyridinic N and pyrrolic N. The incorporation of the active metal phase affects the relative proportions of these species in the final catalysts. In particular, the proportion of pyridinic N is significantly higher in the Pd/C catalyst (58.8%) than in the Pt/C (45.6%) and Au/C (32%) catalysts. Associated with the increased binding energy of Pd 3d caused by the increase of its electronic density, the presence of different proportions of pyridinic N and pyrrolic N reveals that pyridinic N is beneficial for the stabilization of Pd particles on the support. This

beneficial influence accounts for the covalent bonding between pyridine N and Pd particles. For this, the filled π-orbital of pyridine N donates a σ-type covalent bond with partial ionic character to the empty d-orbital of Pd [43]. Therefore, these data indicate that Pd stabilizes better than Pt or Au on the C support.

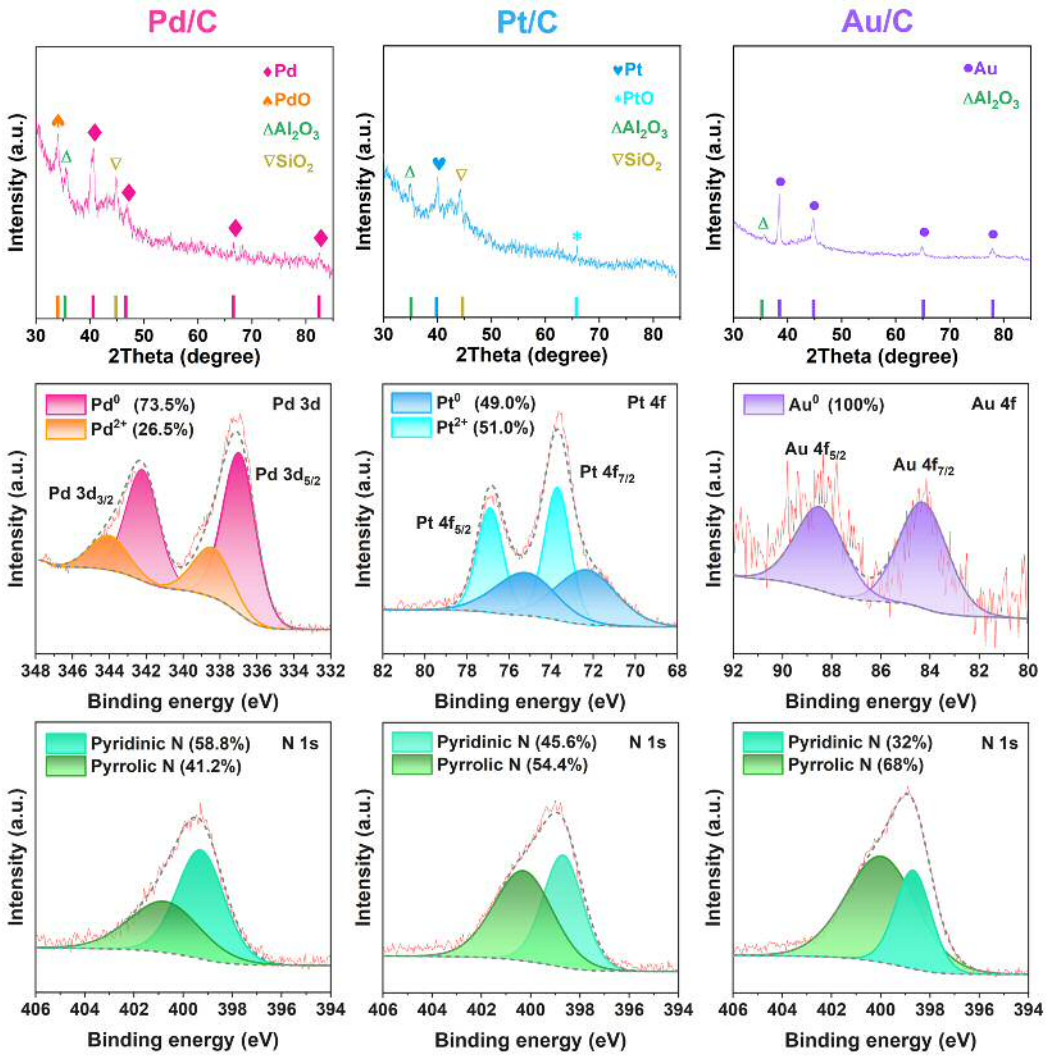

Figure 4. XRD and XPS patterns of Pd/C, Pt/C, and Au/C.

The prepared catalysts were characterized by Raman spectroscopy (Fig. 5) to investigate the degree of graphitization and the presence of defects in the materials. The D band at 1351.2 cm^{-1}

reveals the defect of the internal structure of the carbon material, and the G band at 1593.2 cm^{-1} is related to the plane stretching motion of the sp^2 carbon atom [44]. Regarding the defects and disorder, the ratio between the D and G bands (I_D/I_G) is a helpful parameter for describing the phenomena for carbon materials [45,46]. The I_D/I_G value of the carbon support is 0.96, which increases to 1.02 for Pd/C, 1.01 for Pt/C and 1.03 for Au/C. These results can be ascribed to the disruption in the carbon supports when introducing the active metals, which creates more defects in their structure, thus promoting the catalytic activity.

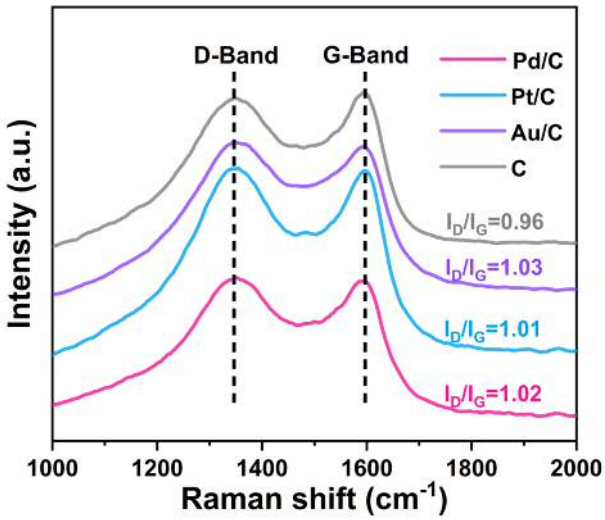

Figure 5. Raman spectra of C, Pd/C, Pt/C, and Au/C.

3.3 Catalytic hydrogenation of vanillin

Preliminarily, the possible catalytic activity of the carbon support was evaluated to address whether or not the support contributes to the catalytic activity of the materials. When the support is used as a catalyst, vanillin conversion is meager, and the liquid product does not contain vanillyl alcohol

(Fig. S3). These data indicate that the carbon support alone is not responsible for the catalytic activity of our metal/C catalysts. The characterization of the liquid effluents produced after the reaction using the Pd/C, Pt/C and Au/C catalysts reveals that they are made up of vanillin, vanillyl alcohol and creosol, without benzene ring-hydrogenated products. The conversion and selectivity to the reaction products are highly dependent on the catalyst. For Pd/C, the conversion of vanillin is as high as 99.9%, with this being converted primarily into vanillyl alcohol (yield of 83.3%), and a small amount (0.2 % yield) of creosol formed. The carbon loss might be attributed to the formation of condensation products that are undetectable by gas chromatography due to their high molecular masses. In comparison, the Pt/C and Au/C catalysts are less catalytically active under the studied conditions. Specifically, the conversions of vanillin are 50.8% and 40.7%, and the yields of vanillyl alcohol are 45.9% and 33.0%, respectively (Fig. 6a). The better catalytic performance of Pd/C can be attributed to two complementary phenomena. On the one hand, Pd-based catalysts are more effective and selective in the hydrogenation of the aldehyde groups in vanillin [32]. The Pd/C catalyst contains both reduced (73.5%) and oxidized (26.5%) species, with a higher proportion of the former and a higher I_D/I_G ratio. In comparison, the Pt/C catalyst contains slightly more oxidized (51.0%) than reduced Pt (49.0%) species, while the Au/C catalyst does not contain oxidized Au species, and both catalysts have lower I_D/I_G ratios. Therefore, the ratio of reduced/oxidized species in the Pd/C catalyst might be a good balance to achieve effective and selective hydrogenation. On the other hand, the higher proportion of pyridinic N in the Pd/C catalyst promotes the stabilization of Pd particles on the carbon support, resulting in a higher catalytic efficiency [47].

Considering the high carbon loss, the reaction conditions of the Pd/C catalyst were optimized to maximize the carbon use efficiency (Fig. 6b-e). Firstly, the catalyst/substrate ratio was decreased to mitigate the condensation reactions. A decrease from 50 mg to 10 mg of catalyst (i.e., a decrease in the catalyst/vanillin ratio from 25 to 5 mg/mmol) in the reaction medium could increase the yield to vanillin alcohol up to 99.3% without compromising the vanillin conversion (99.5%). Secondly, the process was conducted at a milder temperature and the H_2 pressure was reduced to increase the energy efficiency for possible industrial implementation. The experimental results show that the catalyst still displays an excellent catalytic activity. More importantly, vanillin conversions higher than 99% and high vanillyl alcohol yields are achieved even at room temperature (30 ºC) with a H_2 pressure as low as 0.7 MPa. The curves showing the time evolutions of the vanillin conversion and vanillyl alcohol yield overlap, thus demonstrating a high selectivity toward this target product within only 90 min. The ^{1}H and ^{13}C NMR spectra of the hydrogenated products are highly consistent with those of vanillyl alcohol (Fig. 6g). This confirms not only the excellent catalytic performance of Pd/C for the hydrogenation of vanillin to vanillyl alcohol but also the high purity of the vanillyl alcohol produced.

After the optimization, the stability of the Pd/C catalyst was evaluated by recycling experiments (Fig. 6f). The used Pd/C catalyst was separated from the reaction mixture by filtration and desiccated; then, it was used again without any further H_2 reduction. In these experiments, the vanillin conversion and vanillyl alcohol yield remained >99% even after four successive runs. This

indicates that the catalyst is not noticeably deactivated during the process and suggests a high potential for industrial application. Therefore, its catalytic activity was compared with a commercial Pd/C containing 3 wt% of Pd, revealing that our Pd/C catalyst has a significantly superior catalytic performance while the commercial catalyst achieves a substantially lower (34.4%) vanillin conversion. These results highlight the outstanding performance of our Pd/C catalyst and its renewable origin and carbon-neutral nature.

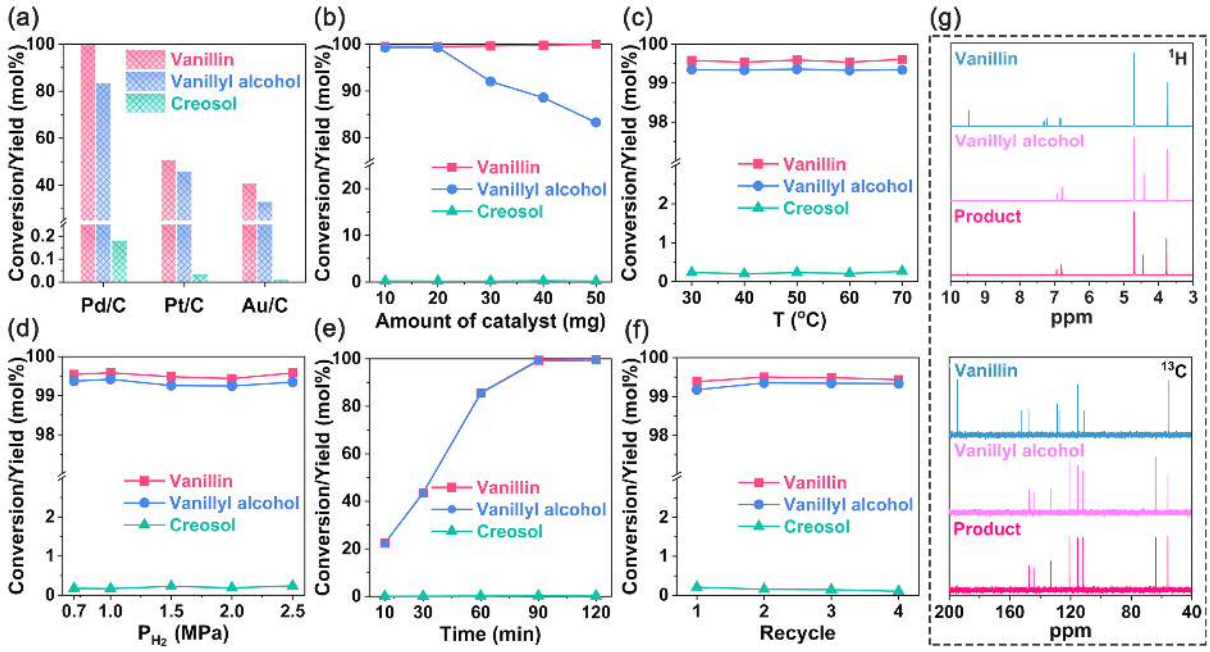

Figure 6. Vanillin hydrogenation reaction (a. Different catalysts; b. Amount of Pd/C; c. Reaction temperature; d. Pressure of H_2; e. Reaction time; f. Stability of the Pd/C.). The 400MHz ^{1}H and ^{13}C NMR spectrums of vanillin, vanillyl alcohol, and the hydrogenated product (g).

3.4 Adsorption performance of the Pd/C catalyst

The adsorption behavior of vanillin and vanillin alcohol on the Pd/C catalyst was investigated to gain more insights into its excellent catalytic performance during the hydrogenation of vanillin to vanillyl alcohol. Their adsorptions capabilities were also compared to those of guaiacol containing the same benzene structure and C-OH and C-O-C functionalities. Under the same conditions, the adsorption performance of the Pd/C is vanillin > guaiacol > vanillyl alcohol (11.5%, 5.8%, and 2.4%, respectively for 2 h adsorption) (Fig. 7). These data indicate that the aldehyde group of vanillin can be readily adsorbed on the Pd/C catalyst, increasing the hydrogenation selectivity of vanillin to vanillyl alcohol. In parallel, the low adsorption of vanillyl alcohol promotes its rapid desorption, avoiding over-hydrogenation and unleashing active catalytic sites on the Pd/C catalyst for further hydrogenation of more vanillin molecules. These results are in close agreement with the high vanillin conversion and vanillyl alcohol selectivity achieved.

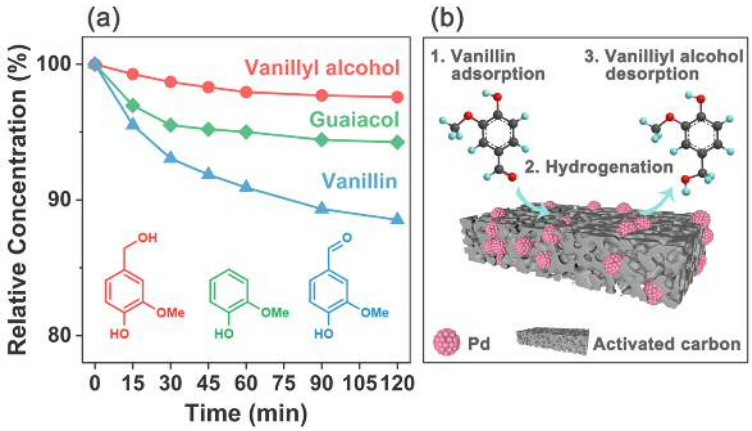

Figure 7. Hydrogenation mechanism of Pd/C (a. Adsorption performance of Pd/C; b. Schematic diagram for hydrogenation of vanillin).

3.5 Catalytic hydrogenation of other lignin-derived aldehydes

The hydrogenation capabilities of the Pd/C catalyst were then tested for the selective hydrogenation of other lignin-derived aldehydes in view of the excellent catalytic features shown for vanillin conversion. Figure 8 shows that our Pd/C catalyst, apart from vanillin, also exhibits an outstanding catalytic performance for the hydrogenation of the aldehyde group into a hydroxymethyl group when p-hydroxybenzaldehyde or syringaldehyde are used as the substrates. In particular, the conversions of p-hydroxybenzaldehyde, vanillin and syringaldehyde are >99% within 60, 90, and 480 min, respectively, with >95% yields to their respective hydrogenated products in all the cases. The varying reaction times needed to complete the process are related to the different hydroxyphenyl (H), guaiacyl (G) and syringyl (S) units in these lignin-derived aldehydes. Their hydrogenation capabilities decrease as follows: H > G > S. These results are attributed to the higher contents of methoxyl groups in G and S units, which can hinder the adsorption of the reactants on the Pd/C catalyst and consequently decelerate the subsequent hydrogenation process.

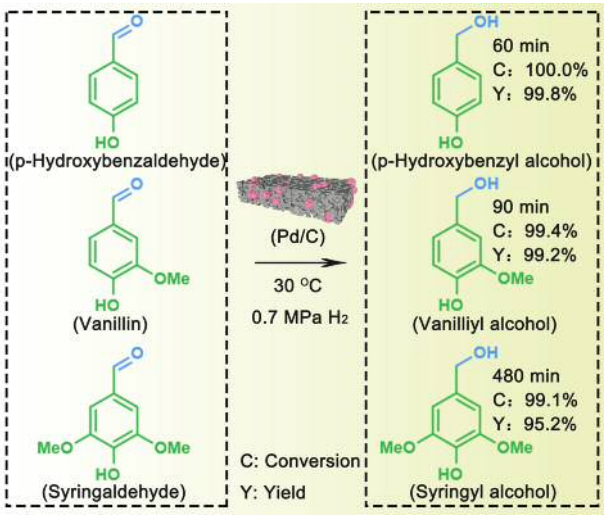

Figure 8. Hydrogenation reactions of other lignin-derived aldehydes.

4 Conclusions

This work has innovated the valorization of a food waste fermentation residue into N-rich Pd/C, Pt/C and Au/C catalysts. These catalysts were tested for the aqueous phase hydrogenation of vanillin to vanillyl alcohol, with the following catalytic activity (based on the vanillin conversion and vanillyl alcohol yield): Pd/C > Pt/C > Au/C. The difference in catalytic performance was related to the higher reduction degree and more pronounced stabilization of the Pd particles on the carbon support compared to those of Pt and Au. The higher ratio of reduced/oxidized metal species and higher ratio of pyridinic N/pyrrolic N of the Pd/C catalyst were also responsible for the superior catalytic performance. The rapid adsorption of the aldehyde group on the Pd/C catalyst, combined with the rapid desorption of the newly formed hydroxymethyl group, also contributed to the excellent activity and selectivity. In particular, at optimum processing conditions (30 ºC and 0.7 MPa H_2 for 90 min, with 2 mmol vanillin/10 mg catalyst), the Pd/C catalyst proved very effective for vanillin hydrogenation with >99% vanillin conversion and vanillyl alcohol selectivity, which could be maintained over four consecutive runs. These results outcompeted those produced with a commercial Pd/C catalyst, which showed substantially lower activity. In addition, the activity of the Pd/C catalyst proved effective for the hydrogenation of other lignin-derived aromatic aldehydes, such as p-hydroxybenzaldehyde and syringaldehyde, into their respective alcohols. These results can promote the selective hydrogenation of lignin-derived aldehydes and

bring novel and promising uses for food waste, thus paving the way for a greener and more sustainable development.

Acknowledgment

This work is financially supported by the National Key R&D Program (2019YFC1906300) and Hong Kong Research Grants Council (PolyU 15222020). We also thank Dr Xiu He at the college of biomass science and engineering, Sichuan University, for experimental assistance. Javier Remón is grateful to the Spanish Ministry of Science, Innovation and Universities for the Juan de la Cierva (JdC) fellowship (Grant Number: IJC2018-037110-I) awarded.

References

[1] M. Melikoglu, C.S.K. Lin, C. Webb. Analysing global food waste problem: Pinpointing the facts and estimating the energy content, Cent. Eur. J. Eng. 3 (2) (2013) 157-164.

[2] Y. Ren, M. Yu, C. Wu, Q. Wang, M. Gao, Q. Huang, Y. Liu. A comprehensive review on food waste anaerobic digestion: Research Updates and Tendencies, Bioresour. Technol. 247 (2018) 1069-1076.

[3] J. Gustavsson, C. Cederberg, U. Sonesson, R.V. Otterdijk, A. Mcybeck. Global food losses and food waste: extent, causes and prevention, Food and Agriculture Organization of the United Nations. (2011).

[4] C.H. Bühlmann, B.S. Mickan, S. Tait, P.A. Bahri. Developing a food waste biorefinery: Lactic acid extraction using anionic resin and impacts on downstream biogas production, Chem. Eng. J. 431 (3) (2022) 133243.

[5] S. Dutta, I.K.M. Yu, J. Fan, J.H. Clark, D.C.W. Tsang. Critical factors for levulinic acid production from starch-rich food waste: Reaction pressure and phase separation, Green Chem. 24 (2022) 163-175.

[6] T.M.W. Mak, X. Xiong, D.C.W. Tsang, I.K.M. Yu, S.P. Chi. Sustainable food waste management towards circular bioeconomy: Policy review, limitations and opportunities, Bioresour. Technol. 297 (2019) 122497.

[7] J. Zhao, Y. Jing, J. Zhang, Y. Sun, Y. Wang, H. Wang, X. Bi. Aged refuse enhances anaerobic fermentation of food waste to produce short-chain fatty acids, Bioresour. Technol. 289 (2019) 121547.

[8] Q. Xu, M. Du, X. Liu, D. Wang, Y. Wu, Y. Li, J. Yang, Q. Fu, D. He, C. Feng, Y. Liu, Q.Wang, B. Ni. Calcium peroxide eliminates grease inhibition and promotes short-chain fatty acids production during anaerobic fermentation of food waste, Bioresour. Technol. 316 (2020) 123947.

[9] G. Strazzera, F. Battista, M. Andreolli, M. Menini, D. bolzonella, S. Lampis. Influence of different household Food Wastes Fractions on Volatile Fatty Acids production by anaerobic fermentation, Bioresour. Technol. 335 (2021) 125289.

[10] S. S. Dhiman, A. David, N. Shrestha, G.R. Johnson, K.M. Benjamin, V. Gadhamshetty, R. K. Sani. Simultaneous hydrolysis and fermentation of unprocessed food waste into ethanol using thermophilic anaerobic bacteria, Bioresour. Technol. 244 (1) (2017) 733-740.

[11] C. Ma, J. Liu, M. Ye, L. Zou, G. Qian, Y. Li. Towards utmost bioenergy conversion efficiency of food waste: Pretreatment, co-digestion, and reactor type, Renew. Sust. Energ. Rev. 90 (2018) 700-709.

[12] Q. Wang, K. Feng, H. Li. Nano iron materials enhance food waste fermentation, Bioresour. Technol. 315 (2020) 123804.

[13] M. He, X. Zhu, S. Dutta, S.K. Khanal, K.T. Lee, O. Masek, D.C.W. Tsang. Catalytic co-hydrothermal carbonization of food waste digestate and yard waste for energy application, Bioresour. Technol. 344 (B) (2022) 126395.

[14] S. Dutta, M. He, X. Xiong, D.C.W. Tsang. Sustainable management and recycling of food waste anaerobic digestate: A review, Bioresour. Technol. 341 (2021) 125915.

[15] A. Ronix, A.L. Cazetta, G.R. Ximenez, L. Spessato, M.C. Silva, J.M. Fonseca, J.T.C. Yokoyama, G.K.P. Lopes, H.G. Zanella, V.C. Almeida. Biochar from the mixture of poultry litter and charcoal fines as soil conditioner: Optimization of preparation conditions via response surface methodology, Bioresour. Technol. Rep. 15 (2021) 100800.

[16] Y. Yang, B. Lin, C. Sun, M. Tang, S. Lu, Q. Huang, J. Yan. Facile synthesis of tailored mesopore-enriched hierarchical porous carbon from food waste for rapid removal of aromatic VOCs, Sci. Total Environ. 773 (2021) 145453.

[17] X. Xiong, I.K.M. Yu, S. Dutta, O. Mašek, D.C.W. Tsang. Valorization of humins from food waste biorefinery for synthesis of biochar-supported Lewis acid catalysts, Sci. Total Environ. 775 (2021) 145851.

[18] J. Liu, R. Ye, J. Shi, H. Wang, L. Wang, P. Jian, D. Wang. Construction of Cu nanoparticles embedded nitrogen–doped carbon derived from biomass for highly boosting the nitrobenzene reduction: An experimental and theoretical understanding, Chem. Eng. J. 419 (2021) 129640.

[19] X. Kong, Y. Zhu, H. Lei, C. Wang, Y. Zhao, E. Huo, X. Lin, Q. Zhang, M. Qian, W. Mateo, R. Zou, Z. Fang, R. Ruan. Synthesis of graphene-like carbon from biomass pyrolysis and its applications, Chem. Eng. J. 399 (2020) 125808.

[20] I.I. Kamińska, E. Kowalewski, D. Lisovytskiy, W. Błachucki, W.R. Pilecka, D. Łomot, A. Śrębowata. Batch and flow hydrotreatment of water contaminated by trichloroethylene on activated carbon supported nickel catalysts, Appl. Catal. A-Gen. 582 (2019) 117110.

[21] F. Hao, J. Zheng, S. He, H. Zhang, P. Liu, H. Luo, W. Xiong. One-step complexed preparation of nitrogen and Cu co-doped oxidative activated carbon catalysts Cu-N/OAC for furfural selective hydrogenation with high yield, Catal. Commun. 151 (2021) 106266.

[22] Q. Lv, W. Si, J. He, L. Sun, C. Zhang, N. Wang, Z. Yang, X. Li, X. Wang, W. Deng, Y. Long, C. Huang, Y. Li. Selectively nitrogen-doped carbon materials as superior metal-free catalysts for oxygen reduction, Nat. Commun. 9 (2018) 3376.

[23] M.A. Mohamed, M.F.M. Zain, L.J. Minggu, M.B. Kassim, J. Jaafar, N.A.S. Amin, M.S. Mastuli, H. Wu, R.J. Wong, Y.H. Ng. Bio-inspired hierarchical hetero-architectures of in-situ

C-doped g-C_3N_4 grafted on C, N co-doped No micro-flowers with booming solar photocatalytic activity, J. Ind. Eng. Chem. 77 (2019) 393-407.

[24] A.A.E. Fakir, Z. Anfar, M. Enneiymy, A. Jada, N.E. Alem. Conjugated copolymer templated carbonization to design n, s co-doped finely tunable carbon for enhanced synergistic catalysis, Appl. Catal. B-Environ. 2021, 120732.

[25] W. Kiciński, M. Szala, M. Bystrzejewski. Sulfur-doped porous carbons: Synthesis and applications, Carbon. 68 (2014) 1-32.

[26] S. Zhou, B. Zhang, Z. Liao, L. Zhou, Y. Yuan. Autochthonous N-doped carbon nanotube/activated carbon composites derived from industrial paper sludge for chromate (VI) reduction in microbial fuel cells, Sci. Total Environ. 712 (2020) 136513.

[27] H. Peng, G. Ma, K. Sun, Z. Zhang, Q. Yang, Z. Lei. Nitrogen-doped interconnected carbon nanosheets from pomelo mesocarps for high performance supercapacitors, Electrochim. Acta. 190 (2016) 862-871.

[28] S. Rawat, P. Gupta, B. Singh, T. Bhaskar, K. Natte, A. Narani. Molybdenum-catalyzed oxidative depolymerization of alkali lignin: selective production of vanillin, Appl. Catal. A-Gen. 598 (2020) 117567.

[29] C. Liao, X. Liu, Y. Ren, D. Gong, Z. Zhang. Catalytic deoxygenation of vanillin over layered double hydroxide supported Pd catalyst, J. Ind. Eng. Chem. 68 (2018) 380-386.

[30] Y. Guo, Y. Hao, Y. Zhou, Z. Han, C. Xie, W. Su, H. Hao. Solubility and thermodynamic properties of vanillyl alcohol in some pure solvents, J. Chem. Thermodyn. 106 (2017) 276-284.

[31] M. Duan, Q. Cheng, M. Wang, Y. Wang. In situ hydrodeoxygenation of vanillin over Ni–Co–P/HAP with formic acid as a hydrogen source, RSC Adv. 11 (2021) 10996-11003.

[32] S. Alijani, S. Capelli, C. Evangelisti, L. Prati, A. Villa, S. Cattaneo. Influence of carbon support properties in the hydrodeoxygenation of vanillin as lignin model compound, Catal. Today. 367 (2021) 220-227.

[33] Y. Chen, X. Li, X. Zheng, D. Wang. Enhancement of propionic acid fraction in volatile fatty acids produced from sludge fermentation by the use of food waste and Propionibacterium acidipropionici, Water Res. 47 (2) (2013) 615-622.

[34] Y. Chen, J. Luo, Y. Yan, L. Feng. Enhanced production of short-chain fatty acid by co-fermentation of waste activated sludge and kitchen waste under alkaline conditions and its application to microbial fuel cells, App. Energy. 102 (2013) 1197-1204.

[35] Y.W. Low, K.F. Yee. A review on lignocellulosic biomass waste into biochar-derived catalyst: Current conversion techniques, sustainable applications and challenges, Biomass Bioenergy. 154 (2021) 106245.

[36] Z. Jiang, M. Gao, W. Ding, C. Huang, C. Hu, B. Shi, D.C.W. Tsang. Selective degradation and oxidation of hemicellulose in corncob to oligosaccharides: From biomass into masking agent for sustainable leather tanning, J. Hazard. Mater. 413 (2021) 125425.

[37] J. Zhang, X. Zhang, G. Xia, Y. Zhang, L. Di. Cold plasma for preparation of Pd/C catalysts toward formic acid dehydrogenation: Insight into plasma working gas, J. Catal. 400 (2021) 338-346.

[38] B. Lin, Y. Zhang, Y. Zhu, Y. Zou, Y. Hu, X. Du, H. Xie, K. Wang, Y. Zhou. Phosphor-doped graphitic carbon nitride-supported Pd as a highly efficient catalyst for styrene hydrogenation, Catal. Commun. 144 (2020) 106094.

[39] R.N.de Andrade, N. Perini, J.L. Vieira, J.M.R. Gallo, E. Sitta. Glycerol electrooxidation catalyzed by Pt-Sb supported in periodic mesoporous carbon CMK-3 and CMK-5, J. Electroanal. Chem. 896 (2021) 115158.

[40] I. Gumus, A. Ruzgar, Y. Karatas, M. Gülcan. Highly efficient and selective one-pot tandem imine synthesis via amine-alcohol cross-coupling reaction catalysed by chromium-based MIL-101 supported Au nanoparticles, Mol. Catal. 501 (2021) 111363.

[41] A.M. Jauhar, Z. Ma, M. Xiao, G. Jiang, S. Sy, S. Li, A. Yu, Z. Chen. Space-confined catalyst design toward ultrafine Pt nanoparticles with enhanced oxygen reduction activity and durability, J. Power Sources. 473 (2020) 228607.

[42] X. Meng, Z. Li, D. Li, Y. Huang, J. Ma, C. Liu, X. Peng. Efficient base-free oxidation of monosaccharide into sugar acid under mild conditions using hierarchical porous carbon supported gold catalysts, Green Chem. 22 (2020) 2588-2597.

[43] J. Yang, X. Qi, F. Shen, M. Qiu, R.L. Smith. Complete dechlorination of lindane over N-doped porous carbon supported Pd catalyst at room temperature and atmospheric pressure, Sci. Total Environ. 719 (2020) 137534.

[44] L. Brownlie, J. Shapter. Advances in carbon nanotube n-type doping: Methods, analysis and applications, Carbon. 126 (2018) 257-270.

[45] M. Ayiania, E. Weiss-Hortala, M. Smith, J.-S. McEwen, M. Garcia-Perez. Microstructural analysis of nitrogen-doped char by Raman spectroscopy: Raman shift analysis from first principles, Carbon. 167 (2020) 559-574.

[46] M.W. Smith, I. Dallmeyer, T.J. Johnson, C.S. Brauer, J.-S. McEwen, J.F. Espinal, M. Garcia-Perez. Structural analysis of char by Raman spectroscopy: Improving band assignments through computational calculations from first principles, Carbon. 100 (2016) 678-692.

[47] M. Dorraj, S. Sadjadi, A. Amani. Pd on a novel nitrogen doped porous carbon derived from task specific ionic liquid and biomass: An efficient catalyst for reduction of organic dyes, Mater. Chem. and Phys. 273 (2021) 124913.